第 30 卷第 6 期 无 机 化 学 学 报 Vol.30 No.6
2014 年 6 月 CHINESE JOURNAL OF INORGANIC CHEMISTRY 1435-1450

# Cu(Ⅱ), Ni(Ⅱ), Co(Ⅱ), Mn(Ⅱ), Zn(Ⅱ)和 Cd(Ⅱ)的乙基 3-(2-氨硫化亚肼基)-2-(羟胺基)丁烯酸酯配合物:合成、表征和细胞毒性

Ramadan M El Bahnasawy[1] Abdou S El-Tabl*,[1] Mohamad M E Shakdofa[2,3]
Noran M Abd El-Wahed[1](埃及)
([1]Chemistry Department, Faculty of Science, Menoufia University, Shebin El-Kom, Egypt)
([2]Chemistry Department, Faculty of Science and Arts, Khulais, King Abdulaziz University) Saudi Arabia)
([3]Inorganic Chemistry Department, National Research Center, P.O. 12622 Dokki, Cairo, Egypt)

**摘要**: 合成了 Cu(Ⅱ),Ni(Ⅱ),Co(Ⅱ),Mn(Ⅱ),Zn(Ⅱ)和 Cd(Ⅱ)的乙基 3-(2-氨硫化亚肼基)-2-(羟胺基)丁烯酸酯配合物($H_2L$)并用元素分析,DTA 热分析,IR,UV-Vis,$^1$H-NMR,质谱,顺磁共振以及磁矩,电导率测量等对合成的配合物进行表征。摩尔电导率测量结果证明合成的配合物为非电解质。光谱数据表明配体分别表现为一元的三齿配体,一元的二齿配体,中性的二齿配体,中性的三齿配体,一元的四齿配体或二元的四齿配体通过席夫碱的氮原子,氨基硫脲中的氮原子,肟中的氮原子和硫酮中的硫原子与金属离子键合生成围绕金属离子的四面体或平面正方形构型。固态 Cu(Ⅱ)(**2**),(**3**),(**4**)和(**5**)的配合物顺磁共振谱表明其为轴向对称,但(**10**~**15**)的配合物却为各向异性。配体和配合物(**2**),(**3**),(**10**),(**13**),(**16**)和(**19**)由于它们对乳腺癌(MCF-7 细胞系)和肝癌(HepG-2 细胞系)的抑制作用而表现出潜在的抗癌活性。

**关键词**: 缩氨基硫脲; 肟; 配合物; 光谱研究; 磁性; 细胞毒性
**中图分类号**: O614.4; O614.121; O614.81+1; O614.81+2; O614.24+1; O614.24+2; O614.71+1 **文献标识码**: A
**文章编号**:1001-4861(2014)06-1435-16
**DOI**:10.11862/CJIC.2014.118

# Cu(Ⅱ), Ni(Ⅱ), Co(Ⅱ), Mn(Ⅱ), Zn(Ⅱ) and Cd(Ⅱ) Complexes of Ethyl-3-(2-carbamothioylhydrazono)-2-(hydroxyimino)butanoate: Synthesis, Characterization and Cytotoxicity Activity

Ramadan M El Bahnasawy[1] Abdou S El-Tabl*,[1] Mohamad M E Shakdofa[2,3] Noran M Abd El-Wahed[1]
([1]*Chemistry Department, Faculty of Science, Menoufia University, Shebin El-Kom, Egypt*)
([2]*Chemistry Department, Faculty of Science and Arts, Khulais, King Abdulaziz University, Saudi Arabia*)
([3]*Inorganic Chemistry Department, National Research Center, P.O.* 12622 *Dokki, Cairo, Egypt*)

**Abstract**: Cu(Ⅱ), Ni(Ⅱ), Co(Ⅱ), Mn(Ⅱ), Zn(Ⅱ) and Cd(Ⅱ) complexes of ethyl-3-(2-carbamo thioylhydrazono)-2-(hydroxyimino)butanoate ($H_2L$) have been synthesized and characterized by elemental and thermal (DTA) analyses, IR, UV-Vis spectroscopy, $^1$H-NMR, mass and ESR spectra as well as magnetic moments, conductivity measurements. The molar conductance measurements indicate that the complexes are non-electrolytes in nature. The spectral data show that the ligand behaves as monobasic tridentate, monobasic bidentate, neutral bidentate, neutral tridentate, monobasic tetradentate or dibasic tetradentate bonded to the metal ions via azomethine nitrogen atom, nitrogen atom of thiosemicarbazide moiety, nitrogen atom of oxime moiety and thione sulphur atom forming

收稿日期:2013-10-17。收修改稿日期:2013-12-25。
*通讯联系人。E-mail:asaeltabl@yahoo.com

octahedral or square planar geometry around the metal ions. The ESR spectra of solid copper(Ⅱ) complexes (**2**), (**3**), (**4**) and (**5**) show axial type symmetry, however, complexes (**10**~**15**) show isotropic type. The ligand and complexes (**2**), (**3**), (**10**), (**13**), (**16**) and (**19**) show potential antitumor activity due to their inhibitory effect on breast carcinoma (MCF-7 cell line) and hepatocellular cancer (HePG-2 cell line).

**Key words**: Thiosemicarbazone, oxime, complexes, spectral studies, magnetism and cytotoxicity activity

## 0 Introduction

Oximes [1-3] and thiosemicarbazones [4-6] are the two important classes of reagents considerable interest because of their chemistry and potentially biological activities. Thiosemicarbazones have a wide range of biological activities such as antitumor [7], antimalarial[8], antileukemic properties [9], antiviral activity [10], antibacterial [11] and antifertility property [12] because of their reduction capability. The thiosemicarbazone moiety is planar and adopts an extended (E) conformation. This planar conformation is due to the extensive electron delocalization throughout the moiety. In general, the N, S-donor ligands of thiosemicarbazones are attributed to their ability to form metal chelates [13]. Oxime metal complexes are biologically active and have been reported to possess semiconducting properties [14]. Also, oximes reveal some interesting features including:

ⅰ-The ability of the oximato group to stabilize higher oxidation states of metals.

ⅱ-The development of bioinorganic models.

ⅲ-The design of selective receptors for Ca(Ⅱ) and Ba(Ⅱ) ions.

ⅳ-The development of new oxygen activation catalysis.

ⅴ-The mechanistic study of corrosion inhibition on iron surfaces.

All these stimulate our interest in metal complexes of oxime ligands. It should be of interest to design, synthesize and use a new type of reagent containing both functional groups viz oxime and thiosemicarbazone. Oxime-Thiosemicarbazone may be considered as functional groups (Two-in-one) viz Oxime and thiosemicarbazone.

## 1 Experimental

### 1.1 Instrumentation

All chemicals and solvents were reagent grade commercial materials and used as received. C, H, N, S and Cl analyses were performed at the Analytical Unit of Cairo University, Egypt. Standard methods were used for determining the metal (Ⅱ) ions [15]. All complexes were dried in vacuo over $P_2O_5$. IR spectra (as KBr pellets) and as Nujol mull between CsBr prisms were recorded on a Perkin-Elmer 581 spectrophotometer (4 000 ~200 $cm^{-1}$). Electronic spectra (qualitative) in the 200~900 nm range were recorded on a Perkin-Elmer 550 spectrophotometer Magnetic susceptibilities were measured at 25 ℃ by the Gouy method using mercuric tetrathiocyanato cobalt (Ⅱ) as the magnetic standard. The magnetic susceptibilities were calculated from the equation $\mu_{eff}=\sqrt{\chi_{M^{Corr}}T}$, where $\chi_{M^{Corr}}$ is the corrected molar susceptibility. Diama gnetic corrections were made using pascal′s constant[16]. Molar conductance were measured on a tacussel type $CD_6NG$ conductivity bridge using $10^{-3}$ mol·$L^{-1}$ DMF. DTA analysis was carried out in air using a Schimadzu DT-30 thermal analyzer. $^1$H-NMR spectra (ligand and its Zn(Ⅱ) complex) were obtained with Bruker Avance 200 MHz spectrometer using $Me_4Si$ as internal standard. Mass spectra (ligand and its Zn(Ⅱ) complex) were recorded using JEULJMS-AX-500 mass spectrometer provided with data system. The ESR spectra of solid complexes at room temperature were recorded using a Varian E-109 spectrometer and DPPH (2,2-diphenyl-1-picrylhydrazyl) was used as the marker. The TLC of the ligand and its complexes confirmed their purity.

### 1.2 Preparation of the ligand

The ligand, ethyl-3-(2-carbamothioylhydrazono)-2-(hydroxyimino) butanoate was prepared by adding dropwise the suspension of thiosemicarbazide (3.14 g, 0.034 mol) in hot 50 $cm^3$ ethanol to the solution of ethyl 2-(hydroxyimino)-3-oxobutanoate (5.0 g, 0.034 mol) in 50 $cm^3$ ethanol (Scheme 1). The mixture was refluxed for 2 h with stirring, then left to cool at room temperature. The yellow precipitate was filtered off, washed with ethanol, dried and recrystallized from ethanol (Scheme 1). Elemental microanalyses. Calcd. for ligand ($H_2L$)=$C_{19}H_{15}N_5O_2$ (FW=232.26): C, 36.20; H, 5.21; N, 24.12, S. 13.81 %. Found: C, 35.78, H, 5.20, N, 23.80; S, 13.51 %. IR data: 3 600, 3 400, 3 250, 1 740, 1 626, 1 612, 1 100, 1 050, 1 018, 875 $cm^{-1}$ assigned to $\nu$(OH, $NH_2$, NH, C=O, C=N, N=C-O, N-OH, C=S). $^1H$ NMR (characterization (DMSO-$d_6$, 200 MHz):=12.90 (s, 1H, OH(**15**)), 7.23 (s, 1H, NH(**4**)), 2.86 (s, 2H, $NH_2$(**1**)), 3.11 (m, 2H, $CH_2$(**13**)), 3.11 (s, 3H, $CH_3$(**7**)), 1.87 (T, 3H, $CH_3$(**14**)), Yield: 75%, Color: yellow. The mass spectrum of the ligand ($H_2L$) reveals molecular ion peak at *m*/*z*=232.

### 1.3 Preparation of metal complexes (2~4), (6), (7), (9-13), (15), (16-20)

A filtered ethanolic (50 $cm^3$) of 0.01 mol metal salts $Cu(CH_3COO)_2\cdot H_2O$ (1.99 g) complex (**2**), $CuCl_2$ (1.70 g) complex (**3**), $Cu(NO_3)_2\cdot 3H_2O$ (2.42 g) complex (**4**), $NiCl_2\cdot 4H_2O$ (2.38 g) complex (**6**), $Ni(CH_3COO)_2\cdot 4H_2O$ (2.49. g) complex (**7**), $Ni(NO_3)_2\cdot 6H_2O$ (2.90 g) complex (**9**), $Co(CH_3COO)_2\cdot 4H_2O$ (2.49 g) complex (**10**), $Co(NO_3)_2\cdot 6H_2O$ (2.91 g) complex (**11**), $CoCl_2\cdot 6H_2O$ (2.38 g) complex (**12**), $MnCl_2\cdot 4H_2O$ (1.97 g) complex (**13**), $Mn(CH_3COO)_2\cdot 4H_2O$ (2.45 g) complex (**15**), $Zn(CH_3COO)_2\cdot 2H_2O$ (2.19 g), complex (**16**), $Zn(NO_3)_2\cdot 6H_2O$ (2.97 g) complex (**17**), $ZnCl_2$ (1.36 g) complex (**18**), Cd $(CH_3COO)_2$ (3.19 g) complex (**19**), $CdCl_2$ (1.83 g) complex (**20**) were added to an ethanolic (50 $cm^3$) of the ligand (**1**) (2.32 g, 0.01 mol) in presence or absence of 3 mL triethyl amine. The mixtures were refluxed with stirring for 3 h. The colored complexes were filtered off, washed several times with ethanol and dried under vacuum over $P_2O_5$. The analytical and physical data are given in Table 1.

### 1.4 Preparation of metal complexes (5), (8), (14)

A filtered ethanolic (50 $cm^3$) of 0.01 mol metal salts $Cu(CH_3COO)_2\cdot H_2O$ (1.99 g) complex (**5**), $Ni(CH_3COO)_2\cdot 4H_2O$ (2.49. g) complex (**8**), $Mn(CH_3COO)_2\cdot 4H_2O$ (2.45 g) complex (**14**), were added to an ethanolic (50 $cm^3$) of the ligand (**1**) (4.64 g, 0.02 mol) in presence or absence of 3 mL triethyl amine. The mixtures were refluxed with stirring for 3 h. The colored complexes were filtered off, washed several times with ethanol and dried under vacuum over $P_2O_5$. The analytical and physical data are given in Table 1.

### 1.5 Biological studies

The cytotoxicity activity was measured in-vitro for the synthesized complexes according to Sulfo-Rhodamine-B-stain (SRB) assay using the published methods against HePG-2 and MCF-7 tumoral cell lines [17]. Cells were plated in 96-multiwell plate ($10^4$ cells/well) for 24 h before treatment with the complexes to allow attachment of cell to the wall of the plate. Different concentrations of the complexes in DMSO (12.5, 25 and 50 $\mu g\cdot mL^{-1}$) were added to the cell monolayer triplicate. Monolayer cells were incubated with the complexes for 48 h at 37°C under atmosphere of 5% $CO_2$. After 48 h, cells were fixed, washed and stained with Sulfo-Rhodamine-B-stain. Excess stain was washed with acetic acid and attached stain was recovered with Tris EDTA buffer (10 mmol·

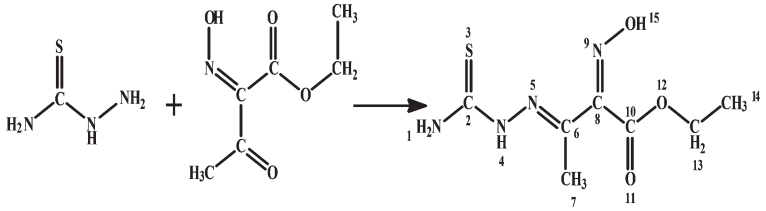


Scheme 1 Synthesis of the ligand $H_2L$ (**1**)

**Table 1 Analytical and physical characteristics for the ligand ($H_2L$) and its complexes**

| No. | Ligand / complexes | Color | m.p. / ℃ | FW | Calcd. (Found) / % | | | | | $\Lambda_M$[a] | Yield / % |
|---|---|---|---|---|---|---|---|---|---|---|---|
| | | | | | C | H | N | S | M | | |
| **1** | $C_7H_{12}N_4O_3S(H_2L)$ | Yellow | 190 | 232.26 | 36.20 (35.78) | 5.21 (5.20) | 24.12 (23.80) | – | – | – | 75 |
| **2** | $[Cu(HL)OAc(H_2O)_2]\cdot H_2O$ | Green | 340 | 407.89 | 26.50 (26.20) | 4.94 (4.70) | 13.74 (13.42) | 7.86 (7.24) | 15.78 (15.51) | 33.5 | 72 |
| **3** | $[Cu(HL)Cl(H_2O)_2]\cdot 2H_2O$ | Brown | 200 | 402.31 | 20.90 (20.56) | 4.76 (4.42) | 13.93 (13.70) | 7.97 (7.56) | 15.80 (15.50) | 30.8 | 70 |
| **4** | $[Cu(HL)NO_3(H_2O)_2]\cdot H_2O$ | Y. Brown | 260 | 428.86 | 19.60 (19.41) | 4.47 (4.11) | 16.33 (16.23) | 7.48 (7.25) | 14.82 (14.58) | 35.3 | 76 |
| **5** | $[Cu(HL)_2]\cdot H_2O$ | Green | 262 | 544.07 | 30.91 (30.55) | 4.45 (4.32) | 20.60 (20.71) | 11.79 (11.33) | 11.68 (11.52) | 36.7 | 71 |
| **6** | $[Ni_2L_2]\cdot H_2O$ | Brown | 268 | 595.89 | 28.22 (27.81) | 3.72 (3.51) | 18.80 (18.62) | 10.76 (10.23) | 19.70 (19.34) | 26.6 | 68 |
| **7** | $[Ni_2(HL)_2(OAc)_2(H_2O)_2]\cdot H_2O$ | Y. Brown | 300 | 752.03 | 28.75 (28.65) | 4.56 (4.32) | 14.90 (14.56) | 8.53 (8.21) | 15.61 (15.28) | 28.6 | 78 |
| **8** | $[Ni(HL)_2(H_2O)_2]\cdot H_2O$ | D. Green | 310 | 575.24 | 29,23 (29.01) | 4.91 (4.88) | 19.48 (19.05) | 11.15 (10.89 | 10.20 (9.85) | 29.2 | 75 |
| **9** | $[Ni(HL)NO_3(H_2O)_2]\cdot H_2O$ | Brown | 210 | 406 | 20.71 (20.52) | 4.22 (4.10) | 17.25 (17.30) | 7.90 (7.45) | 14.46 (14.12) | 28.3 | 72 |
| **10** | $[Co(HL)OAc(H_2O)_2]\cdot 2H_2O$ | Brown | 295 | 421.29 | 25.66 (25.30) | 5.26 (5.00) | 13.30 (13.00) | 7.61 (7.23) | 13.99 (13.80) | 38.3 | 77 |
| **11** | $[Co(H_2L)(NO_3)_2(H_2O)]\cdot 2H_2O$ | Brown | 265 | 469.25 | 17.92 (17.65) | 3.87 (3.71) | 17.91 (17.55) | 6.83 (6.59) | 12.56 (12.44) | 23.8 | 71 |
| **12** | $[Co(H_2L)Cl_2(H_2O)]\cdot 2H_2O$ | D. brown | 280 | 416.15 | 20.20 (19.80) | 4.36 (4.20) | 13.46 (13.13) | 7.71 (6.89) | 14.16 (13.78) | 23.1 | 68 |
| **13** | $[Mn(H_2L)Cl_2(H_2O)]\cdot H_2O$ | D. Brown | 290 | 394.13 | 21.32 (21.11) | 4.09 (3.92) | 14.22 (13.92) | 8.14 (7.87) | 13.94 (13.02) | 23 | 70 |
| **14** | $[Mn(H_2L)_2(OAc)_2]\cdot 2H_2O$ | C. Brown | 330 | 673.58 | 32.10 (29.81) | 5.09 (4.95) | 16.64 (16.12) | 9.52 (9.32) | 8.16 (7.85) | 32.7 | 73 |
| **15** | $[Mn(HL)OAc(H_2O)_2]\cdot H_2O$ | Brown | 285 | 399.28 | 27.07 (26.80) | 5.05 (4.91) | 14.03 (13.71) | 8.03 (7.66) | 13.76 (13.39) | 24.91 | 70 |
| **16** | $[Zn(HL)OAc(H_2O)_2]\cdot H_2O$ | Y. Brown | 295 | 409.75 | 26.38 (26.23) | 4.92 (5.00) | 13.67 (13.54) | 7.83 (7.62) | 15.96 (15.58) | 29.4 | 78 |
| **17** | $[Zn(H_2L)(NO_3)_2(H_2O)]\cdot 3H_3O$ | P. Yellow | 255 | 493.74 | 17.02 (16.83) | 4.08 (3.79) | 17.02 (16.69) | 6.49 (6.51) | 13.25 (13.01) | 37.6 | 70 |
| **18** | $[Zn(HL)Cl]\cdot H_2O$ | White | 290 | 350.13 | 24.01 (23.89) | 3.74 (3.81) | 16.00 (16.11) | 9.16 (9.00) | 18.68 (18.33) | 21.91 | 73 |
| **19** | $[Cd(HL)OAc(H_2O)_2]\cdot H_2O$ | Yellow | 255 | 456.75 | 23.67 (22.53) | 4.41 (4.40) | 12.27 (12.30) | 7.02 (69.86) | 24.61 (25.68) | 33.2 | 75 |
| **20** | $[Cd(H_2L)Cl_2(H_2O)]\cdot 2H_2O$ | Yellow | 295 | 469.62 | 17.90 (17.75) | 3.86 (3.83) | 11.93 (12.31) | 6.83 (6.56) | 23.94 (23.78) | 36.3 | 70 |

$\Lambda_M$[a]=Molar conductivity in $10^{-3}$ mol·L$^{-1}$ solution (S·cm$^2$ ·mol$^{-1}$), Y.=Yellowish, D.=dark, P.=Pale, C.=Cyan

$L^{-1}$ Tris HCl+1 mmol·$L^{-1}$ Disodium EDTA, pH value of 7.5 ~8). Color intensity was measured by ELISA reader. The relation between surviving fraction and complex concentration is plotted to get the survival curve of each tumor cell line after the specified complex treatment.

## 2 Results ad discussion

The analytical and physical data (Tables 1 and 5), and spectral data (Tables 2, 3 and 4) are compatible with the proposed structures (Figures 1, 2 and 3). The complexes are colored, stable in air, insoluble in water

**Table 2 IR spectral ($cm^{-1}$) assignment for the ligand $H_2L$ and their metal complexes**

| No. | ν(OH) | ν($NH_2$) | ν(NH) | ν(C=O) | ν(C=N) | ν(C=N-O) | ν(NOH) | ν($COO^-$) / $NO_3$ | ν(C=S) | ν(M-N) | ν(M-O) | ν(M-S) | ν(M-Cl) |
|---|---|---|---|---|---|---|---|---|---|---|---|---|---|
| **1** | 3 600 | 3 400 | 3 250 | 1 740 | 1626 | 1 612 | 1 100, 1 050, 1 018 | – | 875 | – | – | – | – |
| **2** | – | 3 430 | 3 280 | 1 730 | 1620 | 1 580 | 1 140 | 1 570, 1 465 | 795 | 475 | 610 | 350 | 370 |
| **3** | – | 3 420 | 3 260 | 1 730 | 1620 | 1 592 | 1 145 | – | 796 | 520 | 610 | – | – |
| **4** | – | 3 440 | 3 280 | 1 725 | 1618 | 1 588 | 1 150 | 1 330, 1 260 860,750 | 790 | 512 | 585 | – | – |
| **5** | – | 3 430 | 3 280 | 1 680 | 1622 | 1 585 | 1 168 | – | 790 | 510 | 615 | 315 | 360 |
| **6** | – | 3 400 | 3 250 | 1 680 1 665 | 1610, 1620 | 1 560 | 1 165 | – | 735 | 465 | 605 | 320 | – |
| **7** | – | 3 485 | 3 300 | 1 727 | 1 615 | 1 585 | 1 185, 1 160, 1 140 | 1 556, 1 452 | 860 | 540 | 540 | 360, 350 | – |
| **8** | – | 3 480 | 3 300 | 1 720 | 1 610 | 1 575 | 1 185 | – | 855 | 425 | 630, 605 | – | – |
| **9** | – | – | – | 1 670 | 1615 | 1 610 | 1 165 | 1 380, 1 290, 765,725 | 830 | 465 | 605 | 340 | – |
| **10** | – | 3 780 | 3160 | 1 710 | 1 620 | 1 608 | 1 180 | 1 556, 1 455 | 815 | 510 | 600 | 360 | – |
| **11** | 3 440 | 3 320 | 3170 | 1 700 | 1 610 | – | 1 190, 1 075, 1 007 | 1 390, 1 310, 880, 775 | 845 | 515 | 615 | 325 | – |
| **12** | 3 440 | 3 320 | 3175 | 1 710 | 1 610 | 1 550 | 1 195, 1 080, 1 006 | – | 850 | 515 | 602 | 320 | 430 |
| **13** | 3 575 | 3490 | 3260 | 1 738 | 1 620 | 1 603 | 1 090, 1 045, 1010 | – | 835 | 510 | 585 | 320 | – |
| **14** | 3 550 | 3 460 | 3240 | 1 715 | 1 610, 1 605 | 1 580 | 1 080, 1025, 1005 | 1 550, 1440 | 835 | 552 | 610 | – | – |
| **15** | – | – | – | 1 665 | 1620 | 1 585 | 1 180 | 1 555, 1 445 | 825 | 550 | 615 | 365 | – |
| **16** | 3 560 | 3 380, 3 260 | – | 1 695 | 1 595 | 1 575 | 1 175, 1 140, 1 100, 1 025 | 1 550, 1 370 | 730 | 505 | 565 | 325 | – |
| **17** | 3 560 | 3 400, 3 340 | 3 170 | 1 715 | 1 610 | 1 580 | 1170, 1080, 1 025 | 1 380, 1 315, 870, 760 | 850 | 475 | 610 | 385 | – |
| **18** | – | 3 360 | 3 180 | 1 650 | 1 613 | 1 590 | 1 180, 1 130, 1 080, 1 015 | – | 825 | 615 | – | 325 | 410 |
| **19** | 3 565 | 3 380, 3 275 | – | 1 705 | 1 605 | 1 575 | 1 160, 1 010 1 075 | 1 538, 1 390 | 750 | 505 | 575 | 335 | – |
| **20** | 4 540 | 3 380, 3 260 | 3 180 | 1 740 | 1 615 | 1 595 | 1 245, 1 100, 1 050, 1 010 | – | 840 | 507 | 640 | 340 | 375 |

**Table 3 Electronic absorption spectra and magnetic moments for ligand and its complexes**

| No. | Bands in $CH_3OH$ | Bands / nm | $\mu_{eff}$ / B.M. |
|---|---|---|---|
| **1** | 263 nm ($\varepsilon$=0.34×10$^{-2}$ mol$^{-1}$·cm$^{-1}$), 298 nm ($\varepsilon$=0.38×10$^{-2}$ mol$^{-1}$·cm$^{-1}$), 340 nm ($\varepsilon$=0.35×10$^{-2}$ L·mol$^{-1}$·cm$^{-1}$) | 272, 310, 350 | – |
| **2** | $[Cu(HL)OAc(H_2O)_2]\cdot H_2O$ | 220, 320, 395, 570, 645 | 1.67 |
| **3** | $[Cu(HL)Cl(H_2O)_2]\cdot 2H_2O$ | 222, 260, 395, 495, 590, 630 | 1.65 |
| **4** | $[Cu(HL)NO_3(H_2O)_2]\cdot H_2O$ | 280, 390, 485, 580, 625 | 1.68 |
| **5** | $[Cu(HL)_2]\cdot H_2O$ | 300, 310, 390, 430, 575, 650 | 1.69 |
| **6** | $[Ni_2L_2]\cdot H_2O$ | 290, 360, 405, 520 | Dia. |
| **7** | $[Ni_2(HL)_2(OAc)_2(H_2O)_2]\cdot H_2O$ | 280, 320, 421, 490, 550, 620 | 3.11 |
| **8** | $[Ni(HL)_2(H_2O)_2]\cdot H_2O$ | 250, 300, 495, 540, 590, 650 | 2.98 |
| **9** | $[Ni(HL)NO_3(H_2O)_2]\cdot H_2O$ | 270, 305, 390, 490, 535, 650 | 3.18 |
| **10** | $[Co(HL)OAc(H_2O)_2]\cdot 2H_2O$ | 235, 330, 450, 575, 610 | 4.75 |
| **11** | $[Co(H_2L)(NO_3)_2(H_2O)]\cdot 2H_2O$ | 265, 310, 380, 435, 510, 595, 670 | 4.73 |
| **12** | $[Co(H_2L)Cl_2(H_2O)]\cdot 2H_2O$ | 230, 270, 310, 395, 460, 590, 635 | 4.9 |
| **13** | [Mn(H2L)Cl2(H2O)]·H2O | 216, 310, 395, 430, 560, 615 | 5.6 |
| **14** | $[Mn(H_2L)_2(OAc)_2]\cdot 2H_2O$ | 235, 320, 395, 450, 580, 625 | 5.32 |
| **15** | $[Mn(HL)OAc(H_2O)_2]\cdot H_2O$ | 265, 310, 490, 580, 635 | 5.82 |
| **16** | $[Zn(HL)OAc(H_2O)_2]\cdot H_2O$ | 240, 265, 310, 395 | Dia. |
| **17** | $[Zn(H_2L)(NO_3)_2(H_2O)]\cdot 3H_3O$ | 260, 325, 400 | Dia. |
| **18** | $[Zn(HL)Cl]\cdot H_2O$ | 260, 310, 400 | Dia. |
| **19** | $[Cd(HL)OAc(H_2O)_2]\cdot H_2O$ | 266, 300, 398 | Dia. |
| **20** | $[Cd(H_2L)Cl_2(H_2O)]\cdot 2H_2O$ | 230, 330, 400 | Dia. |

**Table 4 ESR parameter for copper(Ⅱ), cobalt(Ⅱ) and manganese(Ⅱ) complexes**

| No. | $g_{//}$ | $g_{\perp}$ | $^{a}g_{iso}$ | $A_{//(G)}$ | $A_{\perp(G)}$ | $A_{iso}$(G) | $^{b}G$ | $g_{//}/A_{//}$ | $\Delta E_{xy}$ / cm$^{-1}$ | $\Delta E_{xz}$ / cm$^{-1}$ | $\alpha^2$ | $K_{\perp}^2$ | $K_{//}^2$ | $K$ | $\beta^2$ | $\beta_1^2$ | $-2\beta$ | $\alpha^2 d$ / % |
|---|---|---|---|---|---|---|---|---|---|---|---|---|---|---|---|---|---|---|
| **2** | 2.11 | 2.07 | 2.13 | 135 | 15 | 55 | 3.6 | 158.6 | 15 504 | 25 316 | 0.55 | 1.04 | 0.25 | 0.88 | 1.89 | 0.45 | 152 | 64.70 |
| **3** | 2.15 | 2.06 | 2.09 | 140 | 20 | 58.7 | 2.5 | 153.6 | 16949 | 20 202 | 0.6 | 0.7 | 0.38 | 0.77 | 1.17 | 0.63 | 158.9 | 67.60 |
| **4** | 2.2 | 2.08 | 2.12 | 125 | 15 | 51.7 | 2.5 | 169 | 12 741 | 20 618 | 0.63 | 0.97 | 0.51 | 0.9 | 1.53 | 0.81 | 131.8 | 56.10 |
| **5** | 2.16 | 2.05 | 2.09 | 128 | 12 | 50.7 | 3.2 | 166.2 | 17 391 | 23 256 | 0.99 | 0.71 | 0.41 | 0.78 | 0.72 | 0.41 | 140.7 | 59 |
| **10** | | | 2.12 | | | | | | | | | | | | | | | |
| **11** | | | 2.13 | | | | | | | | | | | | | | | |
| **12** | | | 2.11 | | | | | | | | | | | | | | | |
| **13** | | | 2.008 | | | | | | | | | | | | | | | |
| **14** | | | 2.006 | | | | | | | | | | | | | | | |
| **15** | | | 2.05 | | | | | | | | | | | | | | | |

$^{a}g_{iso}=(2\ g_{\perp}+g_{//})/3$, $^{b}G=(g_{//}-2)/(g_{\perp}-2)$

and partially soluble in organic solvents as $CHCl_3$ but soluble in DMF and DMSO. Many attempts have been made to grow single crystal but unfortunately it was failed.

### 2.1 Mass spectra of the ligand (1) and its Zn(Ⅱ) complex (17)

The mass spectrum of the ligand ($H_2L$), (**1**) reveals the molecular ion peak at $m/z$=232 which is coincident with the formula weight 232.26 and supports the identity of the structure. The fragmentation pattern splits a parent ion peak at $m/z$=166 corresponding to $C_3H_6N_3S$ while the fragments at $m/z$ =45 and 104 corresponding to $C_2H_5O$ and $C_3H_6NO_3$, respectively. However Zn(Ⅱ) complex (**17**)

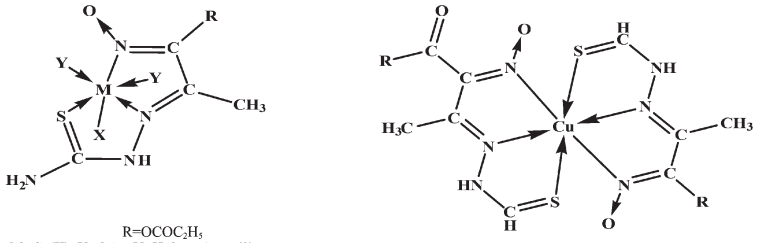

R=$OCOC_2H_5$
M=Cu(II), X=OAc, Y=$H_2O$, *n*=1 (**2**)
M=Cu(II), X=Cl, Y=$H_2O$, *n*=2 (**3**)
M=Cu(II), X=$NO_3$, Y=$H_2O$, *n*=2 (**4**)
M=Ni(II), X=$NO_3$, Y=$H_2O$, *n*=1 (**9**)
M=Co(II), X=OAc, Y=$H_2O$, *n*=2 (**10**)
M=Mn(II), X=OAc, Y=$H_2O$, *n*=1 (**15**)
M=Zn(II), X=Cl, Y=0, *n*=1 (**18**)

$[Cu(HL)_2]\cdot H_2O$
R=$OCOC_2H_5$
(**5**)

Fig.1 Suggested structure of the Cu(Ⅱ), Ni(Ⅱ), Co(Ⅱ), Mn(Ⅱ) and Zn(Ⅱ) complexes (**2**), (**3**), (**4**), (**9**), (**10**), (**15**) and (**18**)

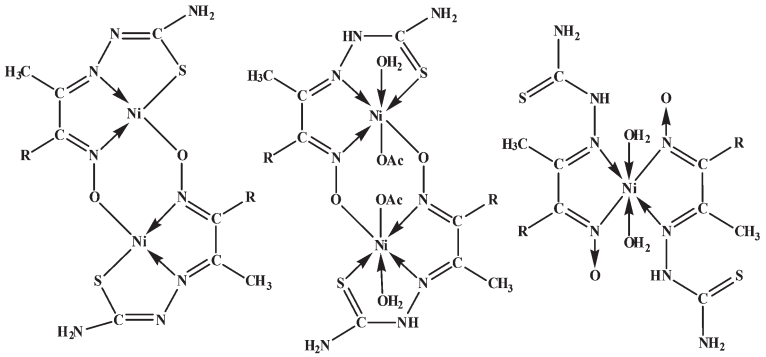

$[Ni_2(L)_2]\cdot H_2O$
R=$OCOC_2H_5$
(**6**)

$[Ni_2(HL)_2(OAc)_2(H_2O)_2]\cdot H_2O$
R=$OCOC_2H_5$
(**8**)

$[Ni(HL)_2(OAc)_2(H_2O)_2]\cdot H_2O$
R=$OCOC_2H_5$
(**8**)

Fig. 2 Suggested structure of the Ni(Ⅱ), complexes (**6**), (**7**), and (**8**)

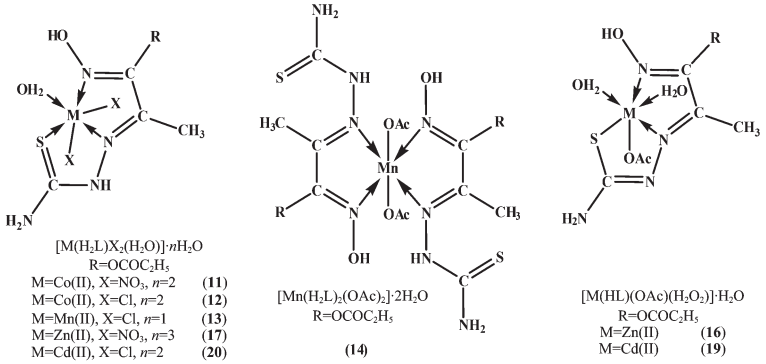

$[M(H_2L)X_2(H_2O)]\cdot nH_2O$
R=$OCOC_2H_5$
M=Co(II), X=$NO_3$, *n*=2 (**11**)
M=Co(II), X=Cl, *n*=2 (**12**)
M=Mn(II), X=Cl, *n*=1 (**13**)
M=Zn(II), X=$NO_3$, *n*=3 (**17**)
M=Cd(II), X=Cl, *n*=2 (**20**)

$[Mn(H_2L)_2(OAc)_2]\cdot 2H_2O$
R=$OCOC_2H_5$
(**14**)

$[M(HL)(OAc)(H_2O_2)]\cdot H_2O$
R=$OCOC_2H_5$
M=Zn(II) (**16**)
M=Cd(II) (**19**)

Fig.3 Suggested structure of the Co(Ⅱ), Mn(Ⅱ), Zn(Ⅱ) and Cd(Ⅱ) complexes (**11**), (**12**), (**13**), (**14**), (**16**), (**17**), (**19**) and (**20**)

shows *m/z* =493 coincident with the formula weight 493.74 a.m.u. The fragments appear at m/z of 73, 116 and 128 are due to $C_3H_5O$, $C_3H_6N_3S$ and $C_4H_6N_3S$, respectively.

## 2.2 Conductivity measurements

The molar conductance values of the complexes in DMF ($10^{-3}$ mol·$L^{-1}$) lie in the 11.91~19.8 S·$cm^2$·$mol^{-1}$ range (Table 1), indicating that all the complexes are not electrolytes[18]. This confirms that the anion is coordinated to the metal ion.

## 2.3 IR spectra

The mode of bonding between the ligand and the metal ion can be revealed by comparing the IR spectra of the solid complexes with that of the ligand. The IR spectral data of the ligand and its metal complexes are presented in Table 2. In principle the ligand can exhibit thione-thiol tautomerism and it contains a thioamide-NH-C=S functional group. The

$\nu$(S-H) band at 2 565 $cm^{-1}$ is absent in the IR spectrum of the ligand but $\nu$(N-H) band at 3 250 $cm^{-1}$ is present, indicating that the ligand remains as the thione tautomer (Scheme 1) in the solid state. The ligand shows two bands in the 3 650~3 300 and 3 280~2 800 $cm^{-1}$ ranges, commensurate the presence of two types of intra- and inter-molecular hydrogen bonds of OH, NH and $NH_2$ groups with imine, thione or carbonyl group[19], thus the higher frequency band is associated with a weaker hydrogen bond and the lower frequency band with a strong hydrogen bond. The medium band at 3 250 $cm^{-1}$ is assigned to $\nu$(NH) group[18-19]. The $\nu$(NH) frequency of $NH_2$ group in the free ligand appears at 3 400 $cm^{-1}$ and not affected by complexation, indicating that, the terminal $NH_2$ group is not involved in the coordination to the metal ion[4]. The band characteristic to carbonyl group $\nu$(C=O) appears at 1 740 $cm^{-1}$, identical to that of the non-coordinated carbonyl group in metal complexes of isonitrosoactylacetone and its derivatives[20-21] and more significantly to the related Schiff base *N*, *N*-diisonitrosoacetylacetonemine 1,2-ethylenediamine and its metal complexes[21-22]. However, the $\nu$(C=N) imine and $\nu$(C=N) oxime are at 1 626 and 1 612 $cm^{-1}$. The oxime bands at 1 100, 1 050 and 1 018 $cm^{-1}$ are assigned to $\nu$(NO)[23-24] and $\nu$(OH) of oxime group appears at 3 600 $cm^{-1}$[23-24]. Strong bands appear in the 3140~2890 $cm^{-1}$ range, are attributed to the $\nu$(CH) vibrations. The band at 875 $cm^{-1}$ is attributed to $\nu$(C=S) vibration[4,25]. The mode of bonding between the ligand and the metal ion can be revealed by comparing the IR spectra of the solid complexes with that of the ligand. By comparing the IR spectra of the complexes (**2**)~(**20**) with that of the free ligand, it is found that the position of $\nu$(C=N) band of thiosemicarbazone is shifted 5~31 $cm^{-1}$ towards lower wavenumber (Table 2) in the complexes, indicating coordination through nitrogen of thiosemicarbazide moiety[4,25]. This is also confirmed by the appearance of new bands in the 615~425 $cm^{-1}$ range, this has been assigned to the $\nu$(M-N)[22]. Strong bands found around 1 100 $cm^{-1}$ in the ligand and its metal complexes is due to $\nu$(N-N) group of the thiosemicarbazone. The position of this band is slightly shifted towards higher wavenumber in the spectra of the complexes; it is due to the increase in the bond strength, which again confirms the coordination via the azomethane nitrogen. The band due to $\nu$(C=S) appears in the 860~790 $cm^{-1}$ range in the complexes shifted to lower wavenumber, indicating that thione sulphur coordinates to the metal ion[22]. Complexes (**16**) and (**19**) show bands at 750 and 730 $cm^{-1}$ which can be assigned to $\nu$(C-S)[4,25]. N-coordination of the oximato group is indicated by $\nu$(C=N) oxime which appears in the 1 610~1 550 $cm^{-1}$ range, the shift of this band to lower wavenumber indicating coordination of nitrogen of oximino group to the metal ion[23-24]. Whereas, the $\nu$(C=O) appears in the 1 740~1 650 $cm^{-1}$ range. These assignments are consistent with those reported for the metal (Ⅱ) complexes of the dioximato ligands [24]. Also, the complexes show $\nu$(N-O) bands in the 1 245~1 100 and 1 090~1 005 $cm^{-1}$ ranges (Table 2), indicating N-coordination of the oximato group[20-21]. Characteristic bands in the 640~540, 615~425 and 385~320 $cm^{-1}$ ranges observed in the complexes may be tentatively assigned to $\nu$(M-O), $\nu$(M-N) and $\nu$(M-S) vibrations, respectively [24]. The strong broad bands in the 3 620~3 090 $cm^{-1}$ are due to hydrated or coordinated water molecules[18], however, broad bands in the 3 650~3 020 and 3 200~2 500 $cm^{-1}$ ranges, are corresponding to intra- and intermolecular hydrogen bonding [19,26]. Complexes (**2**), (**7**), (**10**), (**14**), (**15**), (**16**) and (**19**) show bands in the 1 570~1 538 and 1 465~1 370 $cm^{-1}$ ranges, assigned to the symmetric and asymmetric stretches of the COO group with a $\nu$ value [$\nu(COO)_{asy}-\nu(COO)_{sy}$] more than 100 $cm^{-1}$, which is consistent with the monodentate coordination of carboxylate oxygen[19,27]. Complexes (**4**), (**9**), (**11**) and (**17**) show bands at 1 330, 1 260, 860 and 750, 1 380, 1 290, 765 and 725, 1 390, 1 310, 880 and 775 and 1 380, 1 315, 870 and 760 $cm^{-1}$, respectively which are assigned to the monodentate mode of the nitrate group[24,26]. However, complexes (**3**), (**12**), (**13**), (**18**) and (**20**) show bands at 370, 360, 430, 375 and 410 $cm^{-1}$ are due to $\nu$(M-Cl).

### 2.4 $^1$H-NMR spectra of ligand (1) and its Zn(Ⅱ) complex (17)

The $^1$H-NMR spectrum of the ligand ($H_2L$) in

DMSO-$d_6$ shows signals consistent with the proposed structure (Scheme 1). The peaks observed at 7.23 (s, 1H, NH (**4**)), 2.86 (s, 2H, $NH_2$ (**1**)) are assigned to protons of NH and $NH_2$ groups [19-21]. The signal appeared at 12.90 (s, 1H, OH (**15**)) is assigned to hydroxyl oxime proton[23]. However the signals at 3.11 (m, 2H, $CH_2$(**13**)), 1.87 (T, 3H, $CH_3$(**14**)), 2.33 (s, 3H, $CH_3$ (**7**)) are due to ethoxy and methyl groups respectively [18-19]. Zn (Ⅱ) complex (**20**) shows oxime proton at 12.21 (s, 1H, OH), which appears at lower value indicating coordination of nitrogen oximato group to Zn(Ⅱ) ion. The protons of NH and $NH_2$ groups appear at 7.11 (s, 1H, NH(**4**)), 2.75 (s, 2H, $NH_2$(**1**)), respectively. However the signals at 3.11 (m, 2H, $CH_2$ (**13**)), 2.01 (T, 3H, $CH_3$(**14**)), 3.31 (s, 3H, $CH_3$(**7**)), are due to ethoxy and methyl groups, respectively[18-19].

### 2.5 Magnetic moments

The magnetic moments of metal(Ⅱ) complexes are shown in Table 3. Copper(Ⅱ) complexes (**2**), (**3**), (**4**) and (**5**) show values in the 1.69~1.65 B.M. range corresponding to one unpaired electron in an octahedral geometry around the copper (Ⅱ) ion [19,28]. These values are below the spin only value (1.73 B. M.), indicating that spin- exchange interactions take place between the copper (Ⅱ) ions through hydrogen bonding. Nickel(Ⅱ) complexes (**7**), (**8**), and (**9**) show values 3.11, 2.98 and 3.18 B.M., confirming $T_{2g}{}^6\ell_g{}^2$ electronic configuration with two unpaired electrons in an octahedral nickel (Ⅱ) complexes [21,29], however, complex (**6**) shows a diamagnetic value in accordance with the square planar nickel (Ⅱ) complexes. Manganese(Ⅱ) complexes (**13**), (**14**) and (**15**) show values 5.6, 5.32 and 5.82 B.M. indicating high spin octahedral geometry[18]. Cobalt(Ⅱ) complexes (**10**), (**11**) and (**12**) show values 4.75, 4.92, 4.73 and 4.90 B.M., respectively, indicating high spin octahedral structure [19,25,30]. Zinc(Ⅱ) complexes (**16**)~(**18**) and cadmium(Ⅱ) complexes (**19**) and (**20**) show diamagnetic value.

### 2.6 Electronic spectra

The electronic spectra of the ligand (**1**) and its metal complexes are summarized in Table 3. The spectrum of the ligand in DMF solution exhibits three bands at 263 nm ($\varepsilon$=0.34×10$^{-2}$ L·mol$^{-1}$·cm$^{-1}$), 298 nm ($\varepsilon$=0.38×10$^{-2}$ L·mol$^{-1}$·cm$^{-1}$) and 340 nm ($\varepsilon$=0.35×10$^{-2}$ L·mol$^{-1}$·cm$^{-1}$). The first one may be assigned to $\pi\rightarrow\pi^*$ transition which is nearly unchanged on complexation, whereas the second and third bands are assigned to the $n\rightarrow\pi^*$ and charge transfer transitions of the azomethine, iminoxime and carbonyl groups[31-33]. These bands are shifted to lower energy on complex formation, indicating participation of these groups in coordination with the metal ions or hydrogen bonding formation. In addition, the spectra of the complexes show new bands in 405~395 nm range, which may be attributed to the charge transfer transition [21]. The spectra of copper(Ⅱ) complexes (**2**), (**3**), (**4**) and (**5**) show bands in 265~260, 295~290 and 320~310 nm ranges, these bands are within the ligand, however, the other bands observed in 645~625, 590~570 and 495~465 nm ranges are assigned to $^2B\rightarrow{}^2B_{2g}$, $^2B_{2g}\rightarrow{}^2E_g$ and $^2B_{1B}\rightarrow{}^2A_{1g}$ transitions respectively, indicating tetragonal distorted octahedral geometry[34-35]. Nickel(Ⅱ) complexes (**7**), (**8**) and (**9**) show bands at 770, 620 and 550, 780, 650 and 560, 775, 650 and 535 nm, respectively, corresponding to $^2A_{2g}(F)\rightarrow{}^3T_{2g}(F),(\nu_1)$, $^3A_{2g}(F)\rightarrow{}^3T_{1g}(F),(\nu_2)$, $^3A_{2g}(F)\rightarrow{}^3T_{1g}(P),(\nu_3)$, transitions, indicating octahedral nickel(Ⅱ) complexes[36-37]. The $\nu_2/\nu_1$ ratios are 1.24, 1.20 and 1.19, respectively, which are less than the usual range of 1.5~1.75, indicating distorted octahedral nickel(Ⅱ) complexes[36-37], however, complex (**6**) shows bands at 260, 360, 405, 450 and 520 nm, the first two bands are within the ligand and the other bands are due to $^1A_{1g}\rightarrow{}^1E_g$, $^1A_{1g}\rightarrow{}^1A_{1g}$ and $^1A_{1g}\rightarrow{}^1A_{2g}$ transitions respectively, consistent with square planar geometry[20-21]. Cobalt(Ⅱ) complexes (**10**), (**11**) and (**12**) show bands in 268~260, 310~280, 330, 460~450, 590~575 and 650~610 nm ranges, respectively, the first band is within the ligand and the other bands are assigned to $^4T_{1g}(F)\rightarrow{}^4T_{2g}(P),(\nu_3)$, $^4T_{1g}(F)\rightarrow{}^4A_{2g}(F),(\nu_2)$ and $^4T_{1g}(F)\rightarrow{}^4T_{2g}(F),(\nu_1)$ transitions respectively, corresponding to cobalt(Ⅱ) octahedral structure [31]. The lower value of $\nu_2/\nu_1$ at 1.28 1.22, 1.17 and 1.28 indicates distorted octahedral Co (Ⅱ) complexes [18,30]. Manganese(Ⅱ) complexes (**13**), (**14**) and (**15**) show bands in 265~262, 290~285, 310~320, 450~400, 580~560 and 635~615 nm, ranges, the first three

bands are within the ligand and the other bands are corresponding to $^6A_{1g}\rightarrow{}^4E_g$, $^6A_{1g}\rightarrow{}^4T_{2g}$ and $^6A_{1g}\rightarrow{}^4T_{1g}$ transitions which are compatible to an octahedral geometry around Mn (Ⅱ) ion [38]. However, zinc (Ⅱ) complexes (**16**)~(**18**) and cadmium(Ⅱ), complexes (**19**) and (**20**) show bands in 270~260, 330~270 and 400~395 nm ranges, indicating intraligand transitions within the ligand[39].

### 2.7 Electrons spin resonance (ESR)

The ESR spectral data (Table 4) at room temperature for solid copper(Ⅱ) complexes (**2**), (**3**), (**4**) and (**5**) show the axial type, characteristic of a monomer, $d^9$, configuration with a $d_{x^2-y^2}$ ground state, which is the most common for copper(Ⅱ) complexes[40]. The spectra of these complexes show $g_{//}>g_{\perp}>2.04$, indicating a tetragonal distortion corresponding to elongation along the four fold symmetry axis $z$ [36,41-42]. The $g$-values are related by the expression

$G=(g_{//}-2)/(g_{\perp}-2)$ [43]. If $G>4.0$, then the local tetragonal axes are aligned parallel or only slightly misaligned, if $G<4.0$, the significant exchange coupling is present. The complexes show $G$ value<4.0 (Table 4) indicating spin exchange interactions through hydrogen bonding. Also, these complexes show $g_{//}\leqslant 2.3$, suggesting considerable covalent bond character around the copper(Ⅱ) ion [43-44]. Also, the in-plane -covalence parameter $\alpha^2$(Cu) was calculated by

$$\alpha^2(\mathrm{Cu})=(A_{//}/0.036)+(g_{//}-2.002)+3/7(g_{\perp}-2.002)+0.04 \quad (\mathbf{1})$$

The calculated values (Table 4) suggest covalent bond character [36,45-46]. The $g_{//}/A_{//}$ is taken as an indication for the stereochemistry of the copper (Ⅱ) complexes. Addison [47] has suggested that this ratio may be an empirical indication of the stereochemistry of copper(Ⅱ) complex. The value $g_{//}/A_{//}$ quotient in the 105 ~135 $cm^{-1}$ range is expected for copper (Ⅱ) complexes within perfectly square based geometry and those higher than 150 $cm^{-1}$ for tetragonally distorted octahedral complexes. The values for copper (Ⅱ) complexes (**2**), (**3**), (**4**) and (**5**) are within the range expected for tetragonally distorted complexes. For copper (Ⅱ) complexes with $^2B_1$ ground state, the g-values can be related to the parallel ($K_{//}$) and perpendicular ($K_{\perp}$) components of the orbital reduction factor ($K$) as follows[34-45].

$$K_{//}=(g_{//}-2.002\ 3)\Delta E_{xy}/(8\lambda_o) \quad (\mathbf{2})$$

$$K_{\perp}^2=(g_{\perp}-2.002)\Delta E_{xz}/(2\lambda_o) \quad (\mathbf{3})$$

$$K^2=(K_{//}^2+2K_{\perp}^2)/3 \quad (\mathbf{4})$$

where $\lambda_o$ is the spin orbit coupling of free copper ion, $\Delta E_{xy}$ and $\Delta E_{xz}$ are the electronic transition energies of $^2B_1\rightarrow{}^2B_2$ and $^2B_1\rightarrow{}^2E$, respectively. For the purpose of calculation, it is assumed that the maximum in the band corresponds to $\Delta E_{xy}$, and $\Delta E_{xz}$ can be taken from the wavelength of these bands. From the above relations, the orbital reduction factors ($K_{//}$, $K_{\perp}$ and $K$), a measure of covalency, can be calculated. For an ionic environment $K=1$, and for a covalent environment $K<1$; the lower the value of $K$ (Table 4) shows considerable covalent bond character. The in-plane and out-of-plane $\pi$-bonding coefficients ($\beta_1^2$ and $\beta^2$) are dependent upon the values of $\Delta E_{xy}$ and $\Delta E_{xz}$ in the following equations[44]:

$$\alpha^2\beta^2=(g_{\perp}-2.002)\Delta E_{xy}/(2\lambda_o) \quad (\mathbf{5})$$

$$\alpha^2\beta_1^2=(g_{//}-2.002)\Delta E_{xz}/(8\lambda_o) \quad (\mathbf{6})$$

In this work, the complexes show $\beta_1^2$ values (Table 4), indicating a moderate degree of covalent character in the in-plane $\pi$-bonding, while $\beta^2$ (Table 4), indicating ionic character in the out-of-plane $\pi$-bonding except that complex (**5**) shows covalent character [48-49]. It is possible to calculate the approximate orbital population for d orbital using the following equations[40].

$$A_{//}=A_{iso}-2B(1\pm 7/4)\Delta g_{//} \quad (\mathbf{7})$$

$$a_d^2=2B/2B^\circ \quad (\mathbf{8})$$

where $2B^\circ$ is the calculated dipolar coupling for unit occupancy of the $d$ orbital. When the data of complexes are analyzed, the results suggest an orbital population close to 67.6% ~59% range of $d$-orbital spin density (T able 4) clearly, the orbit of the unpaired electron is a $d_{x^2-y^2}$ orbit[19]. The ESR spectra for manganese(Ⅱ) complexes (**13**)~(**15**) and cobalt(Ⅱ) complexes (**10**)~(**12**) show isotropic type indicating octahedral geometry around Mn (Ⅱ) and Co (Ⅱ) ions, respectively[50].

### 2.8 Thermal analysis (DTA)

Since the IR spectra indicate the presence of

water molecules, thermal analysis (Table 5) was carried out to ascertain their nature. The DTA curves in the temperature 27~800 ℃ range for complexes (**2**)~(**20**) show that the complexes are thermally stable up to 60 ℃. Also, the results show that, the complexes loose hydrated water molecules in the 60~90 ℃ range, this process is accompanied by an endothermic peak. The coordinated water molecules are eliminated at relatively higher temperature than those of the hydrated water molecules (135~265 ℃) (Table 5),

**Table 5 Thermal analysis (DTA) of complexes**

| Comp. No. | Temp. / ℃ | DTA / (peak) | Assignment |
|---|---|---|---|
| **2** | 60 | Endo. | Dehydration process ($H_2O$) |
| | 235 | Exo. | Loss of coordinated water ($2H_2O$) |
| | 300 | Endo. | Loss of one acetate ions ($CH_3COOH$) |
| | 450, 500, 600 | Exo. | Decomposition with the formation of CuO |
| **3** | 70 | Endo. | Dehydration process ($2H_2O$) |
| | 185 | Exo. | Loss of coordinated water ($2H_2O$) |
| | 200 | Endo. | Melting point |
| | 265 | Endo. | Loss of one chloride ion (HCl) |
| | 450, 600 | Exo. | Decomposition with the formation of CuO |
| **4** | 60 | Endo. | Dehydration process ($2H_2O$) |
| | 155 | Endo. | Loss of coordinated water ($2H_2O$) |
| | 230 | Exo. | Melting point |
| | 260 | Endo. | Loss of one nitrate ion ($HNO_3$) |
| | 450, 500, 650 | Exo. | Decomposition with the formation of CuO |
| **5** | 65 | Endo. | Dehydration process ($H_2O$) |
| | 262 | Endo. | Melting point |
| | 350, 465, 615 | Exo. | Decomposition with the formation of CuO |
| **6** | 95 | Endo. | Dehydration process ($H_2O$) |
| | 268 | Endo. | Melting point |
| | 350, 450, 600, 670 | Exo. | Decomposition with the formation of $Ni_2O_3$ |
| **7** | 65 | Endo. | Dehydration process ($H_2O$) |
| | 265 | Endo. | Loss of coordinated water ($2H_2O$) |
| | 300 | Endo. | Melting point |
| | 360, 475, 510, 660 | Exo. | Decomposition with the formation of NiO |
| **8** | 65 | Endo | Dehydration process ($H_2O$) |
| | 175 | Endo. | Loss of coordinated water ($2H_2O$) |
| | 290 | Endo. | Phase transformation |
| | 310 | Endo. | Melting point |
| | 450, 510, 670 | Exo. | Decomposition with the formation of NiO |
| **9** | 90 | Endo. | Dehydration process ($2H_2O$) |
| | 150 | Endo. | Loss of coordinated water ($2H_2O$) |
| | 210 | Endo. | Melting point |
| | 270 | Endo. | Loss of one nitrate ion ($HNO_3$) |
| | 350, 500, 550, 670 | Exo. | Decomposition with the formation of NiO |
| **10** | 75 | Endo. | Dehydration process ($2H_2O$) |
| | 190 | Endo. | Loss of coordinated water ($2H_2O$) |
| | 295 | Endo. | Melting point |
| | 310 | Endo. | Loss of one acetate ions ($CH_3COOH$) |
| | 390, 480, 600 | Exo. | Decomposition with the formation of CoO |

Continued Table 5

| | | | |
|---|---|---|---|
| **11** | 90 | Endo. | Dehydration process ($2H_2O$) |
| | 165 | Endo. | Loss of coordinated water ($H_2O$) |
| | 265 | Endo. | Melting point |
| | 325 | Endo. | Loss of two nitrate ions ($HNO_3$) |
| | 450,520,660 | Exo. | Decomposition with the formation of CoO |
| **12** | 90 | Endo. | Dehydration process ($2H_2O$) |
| | 180 | Endo. | Loss of coordinated water ($H_2O$) |
| | 280 | Endo. | Melting point |
| | 320 | Endo. | Loss of two chloride ion (HCl) |
| | 430, 460, 550, 650 | Exo. | Decomposition with the formation of CoO |
| **13** | 80 | Endo. | Dehydration process ($H_2O$) |
| | 165 | Endo. | Loss of coordinated water ($H_2O$) |
| | 205 | Endo. | Phase transformation |
| | 290 | Endo. | Melting point |
| | 380,465,590 | Exo. | Decomposition with the formation of MnO |
| **14** | 65–80 | Endo. . | Dehydration process ($H_2O$) |
| | 330 | Endo. | Melting point |
| | 395.470.640 | Exo. | Decomposition with the formation of MnO |
| **15** | 80 | Endo. | Dehydration process ($H_2O$) |
| | 165 | Endo. | Loss of coordinated water ($2H_2O$) |
| | 285 | Endo. | Melting point |
| | 350,510,615 | Exo. | Decomposition with the formation ofb MnO |
| **16** | 75 | Endo. | Dehydration process ($H_2O$) |
| | 175 | Endo. | Loss of coordinated water ($2H_2O$) |
| | 275 | Endo. | Melting point |
| | 305, 450, 560, 650 | Exo. | Decomposition with the formation of ZnO |
| **17** | 85~95 | Endo. | Dehydration process ($3H_2O$) |
| | 185 | Endo. | Loss of coordinated water ($H_2O$) |
| | 255 | Endo. | Melting point |
| | 350 | Endo. | Loss of two nitrate ions ($HNO_3$) |
| | 450, 550, 650 | Exo. | Decomposition with the formation of ZnO |
| **18** | 85 | Endo. | Dehydration process ($H_2O$) |
| | 290 | Endo. | Melting point |
| | 325 | Endo. | Loss of one chloride ion (HCl) |
| | 450.560,650 | Exo. | Decomposition with the formation of ZnO |
| **19** | 70 | Endo. | Dehydration process ($H_2O$) |
| | 135 | Endo. | Loss of coordinated water ($2H_2O$) |
| | 255 | Endo. | Melting point |
| | 300 | Endo. | Loss of one acetate ion ($CH_3COOH$) |
| | 370, 465, 550, 660 | Exo. | Decomposition with the formation of CdO |
| **20** | 80 | Endo. | Dehydration process ($2H_2O$) |
| | 150 | Endo. | Loss of coordinated water ($H_2O$) |
| | 290 | Endo. | Melting point |
| | 315 | Endo. | Loss of two chloride ions (HCl) |
| | 375, 450, 530, 650 | Exo. | Decomposition with the formation of CdO |

which are accompanied by endothermic peaks[33,49,51-52]. The removal of acetate ion as $CH_3COOH$ molecule accompanied by an endothermic peak is observed for complexes (**2**), (**10**) and (**19**) in the 300~352 ℃ range. Complexes (**3**), (**12**), (**18**) and (**20**) lose chloride ion as HCl with endothermic peak in the 265~325 ℃ range. However, complexes (**4**), (**9**), (**11**) and (**17**) lose nitrate group as $HNO_3$ with endothermic peak in the 260~350 ℃ range. The complexes show an endothermic peak within 200~340 ℃ range is due to melting of the complexes. The complexes show exothermic peaks within 350~670 ℃ range (Table 5) corresponding to oxidative thermal decompositions, which proceeds slowly with a final residue, leaving metal oxides[52]. The thermal decomposition of complex (**2**) can be represented as follows:

$$[(HL)Cu(OAc)(H_2O_2)]\cdot H_2O \rightarrow [(HL)Cu(OAc)(H_2O_2)]+H_2O \quad (\mathbf{9})$$

$$[(HL)Cu(OAc)(H_2O_2)_2] \rightarrow [(HL)Cu(OAc)]+2H_2O \quad (\mathbf{10})$$

$$[(HL)Cu(OAc)] \rightarrow [(L)Cu]+CH_3COOH \quad (\mathbf{11})$$

$$[(L)Cu] \rightarrow CuO \quad (\mathbf{12})$$

### 2.9 *In-vitro* cytotoxicity

The *in-vitro* cytotoxicity properties of the oxime thiosemicarbazone ligand (**1**) and its metal complexes (**2**), (**3**), (**10**), (**13**), (**16**) and (**19**) were evaluated against MCF-7 and HePG-2 tumoral cell lines. The ligand (**1**) shows a weak inhibition effect at ranges of concentration used, however, the complexes show moderate and almost similar behavior. This property may be due to the same coordination sites (N, O and S donor atoms) and the same geometry (octahedral) around the metal(Ⅱ) ion. The data indicate that the surviving fraction ratio against MCF-7 or HePG-tumor cell lines increases with the increase of the concentration. Also, the complexes show a high potency around 80% inhibition at 50 $\mu g\cdot mL^{-1}$ against MCF-7, or HePG-2 compared with standard drugs (Tamoxifen and Sorafenib). It seems that the change in the anion and the nature of the metal ion has effect on the biological behavior in complexes, which could be explained by Tweedy′s chelation theory [53-58]. To understand the mechanism involved in these processes. Copper (Ⅱ) complexes would cause intracellular generation of hydroxyl radical OH from $H_2O_2$ produced during normal cellular activities by the reduction of Cu(Ⅱ) to Cu(Ⅰ) ion leading to growth inhibition on tumor cell[59]. The decomposition of $H_2O_2$ in the presence of Cu(Ⅱ) complex may be represented as follows[60].

$$H_2O_2 \rightarrow H^+, HO^- \rightarrow HO_2+e \quad (\mathbf{13})$$

$$Cu(Ⅱ)+e \rightarrow Cu(Ⅰ), Cu(Ⅰ) \rightarrow Cu(Ⅱ)+e \quad (\mathbf{14})$$

$$H^++e \rightarrow H, H_2O_2 \rightarrow H_2O+1/2O_2 \quad (\mathbf{15})$$

$$H_2O_2 \rightarrow OH\cdot+OH\cdot, 2e+H_2O \rightarrow HO_2+e \quad (\mathbf{16})$$

$$OH^- \rightarrow OH+e, 4OH \rightarrow 2H_2O+O_2 \quad (\mathbf{17})$$

$$H^++e+H_2O \rightarrow H_2+OH^- \quad (\mathbf{18})$$

Moreover, Gaetke and Chow [61] reported that copper facilitated oxidated tissue injury through a free-radical mediated pathway analogous to the Fenton reaction. By applying the ESR-trapping technique, evidence for copper-mediated hydroxyl radical formation in-vivo has been obtained[61]. Radicals are produced through a Fenton-type reaction as follows:

$$LCu(Ⅱ)+H_2O_2 \rightarrow LCu(Ⅰ)+{}^-OOH+H^+ \quad (\mathbf{19})$$

$$LCu(Ⅰ)+H_2O_2 \rightarrow LCu(Ⅱ)+\cdot OH+OH^- \quad (\mathbf{20})$$

where L=organic ligand

Also, copper could act as a double-edged sword by inducing DNA damage and also by inhibiting their repair[62]. The OH radicals react with DNA sugars and bases, and the most significant and well-characterized

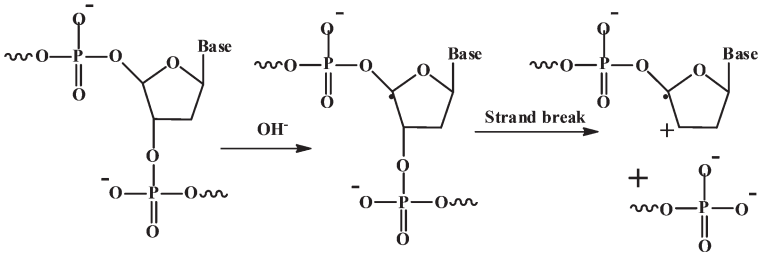


Scheme 2 Suggested mechanism for OH radicals attack on DNA sugars and bases

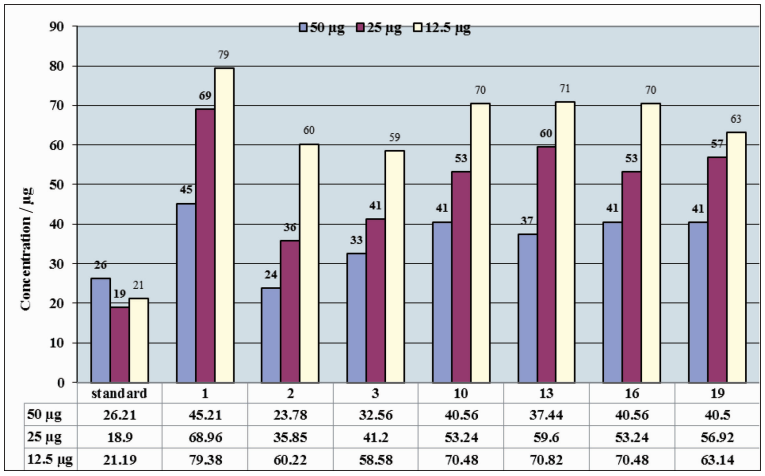


| | standard | 1 | 2 | 3 | 10 | 13 | 16 | 19 |
|---|---|---|---|---|---|---|---|---|
| 50 µg | 26.21 | 45.21 | 23.78 | 32.56 | 40.56 | 37.44 | 40.56 | 40.5 |
| 25 µg | 18.9 | 68.96 | 35.85 | 41.2 | 53.24 | 59.6 | 53.24 | 56.92 |
| 12.5 µg | 21.19 | 79.38 | 60.22 | 58.58 | 70.48 | 70.82 | 70.48 | 63.14 |

Fig.4 Cytotoxicity of standard, ligand (**1**) and complexes (**2**), (**3**), (**10**), (**13**), (**16**) and (**19**) against HEPG-2 liver cell

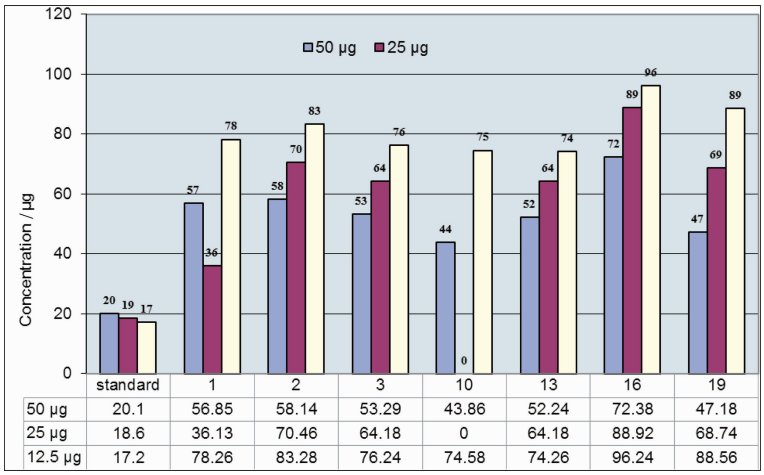


| | standard | 1 | 2 | 3 | 10 | 13 | 16 | 19 |
|---|---|---|---|---|---|---|---|---|
| 50 µg | 20.1 | 56.85 | 58.14 | 53.29 | 43.86 | 52.24 | 72.38 | 47.18 |
| 25 µg | 18.6 | 36.13 | 70.46 | 64.18 | 0 | 64.18 | 88.92 | 68.74 |
| 12.5 µg | 17.2 | 78.26 | 83.28 | 76.24 | 74.58 | 74.26 | 96.24 | 88.56 |

Fig.5 Cytotoxicity of standard, ligand (**1**) and complexes (**2**), (**3**), (**10**), (**13**), (**16**) and (**19**) against MCF-7 cell

OH reactions are hydrogen atom abstraction from the $C_4$ on the deoxyribose unit to yield sugar radicals with subsequent $\beta$-elimination (Scheme 2). By this mechanism, strand breakage occurs as well as the release of the free bases. Another form of attack on the DNA bases is by solvated electrons, probably via a similar reaction to those discussed below for the direct effects of radiation on DNA[62].

The cytotoxicity of a standard drug, ligand and its complexes at the range of concentrations used against human HePG-2 cell lines and MCF-7 breast cancer are shown in Figures (4) and (5).

## 3 Conclusions

New copper(Ⅱ), nickel(Ⅱ), cobalt(Ⅱ), manganese(Ⅱ), zinc (Ⅱ) and cadmium (Ⅱ) of ethyl-3-(2-carbamothioylhydrazono)-2-(hydroxyimino)butanoate have been designed, synthesized, and characterized using different spectroscopic and analytical techniques. Comparison of the IR spectra of the ligand and their metal complexes indicate that the oxime acts as monobasic tridentate, monobasic bidentate, neutral bidentate, neutral tridentate, monobasic tetradentate or dibasic tetradentate bonded to the metal ions via azomethine nitrogen atom, nitrogen atom of thiosemicarbazide moiety, nitrogen atom of oxime moiety and thione sulphur atom forming octahedral or square planar geometry around the metal ions. The *in-vitro* cytotoxicity activities of the ligand and its complexes against the growth tumor cell lines MCF-7 and HePG-2 tumoral cell lines indicate that the ligand shows weak inhibition effect at ranges of concentration

used, however, the complexes show moderate and almost similar behavior. This cytotoxicity activities may be due to the same coordination sites (N, O and S donor atoms) and the same geometry (octahedral) around the metal(Ⅱ) ion.

## References:

[1] Kurtolu M, Dadelen M M, Torlu S. *Trans. Met. Chem.*, **2006**,**31**(3):382-388
[2] Hsieh W Y, Liu S. *Inorg. Chem.*, **2006**,**45**:503-504
[3] Aly M M, El-Said F A. *J. Inorg. Nucl. Chem.*, **1981**,**43**(2): 287-292
[4] El-Tabl A S, Ayad M I. *Synth. React. Inorg. Met. Org. Chem.*, **2003**,**33**:369-385
[5] Kasuga N C, Onodera K, Nakano S, et al. *J. Inorg. Biochem.*, **2006**,**100**(7):1176-1186
[6] Otero L, Folch C, Barriga G, et al. *Spectrochem. Acta Part A*, **2008**,**70**(3):519-523
[7] Offiong O E, Martelli S. *Trans. Met. Chem.*, **1997**,**22**(3):263-269
[8] Scovill J P, Klayman D L, Lambros C, et al. *J. Med. Chem.*, **1984**,**27**(11):87-91
[9] Scovill J P, Klayman D L, Franchino C F. *J. Med. Chem.*, **1983**,**25**(10):1261-1264
[10]Rasman J, Heinisch G, Holzer W, et al. *J. Med. Chem.*, **1992**,**35**(17):3288-3296
[11]Dobek A S, Klayma D L, Dickson E T, et al. *Antimicrob. Agents Chemother.* **1980**,**18**(1):27-36
[12]Shetti S N, Murty A S. *Trans. Met. Chem.*, **1993**,**18**(5):467-472
[13]Reddy K H, Reddy D V. *Anal. Lett.*, **1984**,**17** (11):1275-1291
[14]Özcan E, Karapinar E, Demirtas B. *Trans. Met. Chem.*, **2002**,**27**(5):557-561
[15]Vogel AI. *A Text Book of Quantitative Inorganic Analyses*. 2*nd Ed*., London: Longman, **1951**.
[16]Lewis J, Wilkins R G. *Modern Coordination Chemistry*. New York: Interscience, **1960**:403
[17]Skehan P, Storeng R. *J. Natl. Cancer Inst.*, **1990**,**82**:1107-1112
[18]Geary W J. *Coord. Chem. Rev*., **1971**,**7**:81-122
[19]El-Tabl A S, El-Saied F A, Al-Hakim A N. *Trans. Met. Chem*., **2007**,**32**(6):689-701
[20]Aly M M, Imam S M. *Monatsh. Chem*., **1995**,**126**(2):137-147
[21]Aly M M, Baghlaf A O, Ganji N S. *Polyhedron*, **1985**,**4**(7): 1301-1309
[22]Aly M M, Al-Sharri N I. *Trans. Met. Chem.*, **1998**,**23**(4):361-369
[23]Plass W, El-Tabl A S, Pohmann A. *J. Coord. Chem.*, **2009**, **62**(10):258-372
[24]El-Tabl A S. *Trans. Met. Chem*., **2002**,**27**(2):166-170
[25]El-Tabl A S, Kashar T I, El-Bahnasawy R M, et al. *Polish J. Chem*., **1999**,**73**(2):245-254
[26]Nakamoto K. *Infrared Spectra of Inorganic and Coordination compounds*. New York: Wiley, **1970**.
[27]Abu El-Reash G M, Ibrahim K M, Bekheit M M. *Trans. Met. Chem*., **1990**,**15**(2):148-151
[28]Youssef N S, Hegab K H. *Synth. React. Inorg. Met. Org. Nano-Met. Chem*., **2005**,**35**(5):391-399
[29]El-Tabl A S, El-Bahnasawy R M, Shakdofa M M E, et al. *J. Chem. Res*., **2010**,**49**:88-91
[30]Al-Hakimi A N, Shakdofa M M E, El-Seidy A M, et al. *J. Korean. Chem. Soc*., **2011**,**55**(3):418-429
[31]Dongli C, Handong J, Hongyun Z, et al. *Polyhedron*, **1994**, **13**(1):57-62
[32]El-Motaleb A, Gaber M. *Trans. Met. Chem*., **1997**,**22**(3):211-215
[33]El-Tabl A S. *J. Chem. Reas*., **2002**(11):529-531
[34]Bao S Q, Lin L Z, Li W X, et al. *Trans. Met. Chem*., **1994**,**19**(5):503-505
[35]Sreeja P B, Kurup M R P, Kishore A C. *Polyhedron*, **2004**,**23**(4):575-581
[36]Bigatto A B, Costa G, Galasso V, et al. *Spectrochim. Acta*, **1970**,**26**(9):1939-1949
[37]Mohamed G G, Omar M M, Hindy A M M. *Spectrochim. Acta*, Part A, **2005**,**62**(4):1140-1150
[38]Parihari R K, Patel R K, Patel R N. *J. Ind. Chem. Soc*., **2000**,**77**:339-341
[39]Krishna C H, Mahapatra C M, Dush K C. *J. Inorg. Nucl. Chem*., **1987**,**39**:1253-1258
[40]El-Tabl A S. *Trans. Met. Chem*., **1997**,**22**(4):400-405
[41]Lever A B P. *Inorganic Electronic Spectroscopy*. New York: Elsevier, **1968**:335
[42]Figgs B N, Lewis J. *Prog. Inorg. Chem.*, **1967**,**6**:37-39
[43]El-Tabl A S, Plass W, Buchnolz A, et al. *J. Chem. Res*., **2009**:582-587
[44]E-Tabl A S. *Trans. Met. Chem*., **1996**,**21**(1):1-4
[45]Procter I M, Hathaway B J, Nicholls P. *J. Chem. Soc. A*, **1969**:1678-1684
[46]Kivelson D, Neiman R. *J. Chem. Phys*., **1961**,**35**(1):149-155
[47]El-Tabl A S, Shakdofa M M, El-Seidy A M A, et al. *J. Korean Chem. Soc*., **2010**,**55**(1):19-27
[48]Addison A W. *Copper Coordination Chemistry: Biochemical,*

*Inorganic Perspectives*. New York: Adenine Press, **1983**.

[49]Shauib N M, Elassar A Z, El-Dissovky A. *Spectrochim. Acta*, Part A, **2006**,**63**(3):714-722

[50]Kuska H A, Rogers M T. *Coordination Chemistry*. Martell A E, Ed. New York: Van Nostrand Reinhold, **1971**.

[51]Bhadbhade M M, Srinivas D. *Inorg. Chem*., **1993**,**32** (24): 5458-5466

[52]El-Tabl A S. *Bull. Korean Chem. Soc*., **2004**,**25** (12):1757-1763

[53]El-Tabl A S, Abou-Sekkina M M. *Polish J. Chem*., **1999**,**73** (12):1937-1953

[54]Illan N A, Garcia A R, Moreno M, et al. *J. Inorg. Biochem.*, **2005**,**99**(8):1637-1645

[55]Hall I H, Leem C C, Ibrahim G, et al. *Appl. Oranomet. Chem.*, **1997**,**11**(7):565-575

[56]Feng G, Mareque-Rivas J C, Rosales R T, et al. *J. Am. Chem. Soc*., **2005**,**127**(39):13470-13471

[57]Mareque J C, Prabaharan R, Parsons S. *Dalton Trans.*, **2004**:1648-1655

[58]Bauer-Siebenlist B, Meyer F, Farakas E, et al. *J. Chem. Eur.*, **2005**,**11**(15):4349-4360

[59]Kadiiska M B, Mason R P. *Spectrochim. Acta, Part A*, **2002**,**58**(6):1227-1239

[60]El-Boraey H A, El-Tabl A S. *Polish J. Chem*., **2003**,**77**(12): 1759-1776

[61]Gaetke L M, Chow C K. *Toxicology*, **2003**,**189** (1/2):147-163

[62]Rouzer C A. *Chem. Res. Toxicol*., **2010**,**23**(10):1517-1518